Published in final edited form as:
Br J Ophthalmol. 2010 March ; 94(3): 372–376. doi:10.1136/bjo.2009.163501.

Retinal imaging using commercial broadband optical coherence tomography

Hitesh Tanna[1], **Adam M Dubis**[2], **Nazia Ayub**[3], **Diane M Tait**[3], **Jungtae Rha**[3], **Kimberly E Stepien**[3], and **Joseph Carroll**[2,3,4]

[1]Department of Biomedical Engineering, Medical College of Wisconsin, Marquette University, Milwaukee, Wisconsin, USA

[2]Department of Cell Biology Neurobiology, & Anatomy, Medical College of Wisconsin, Milwaukee, Wisconsin, USA

[3]Department of Ophthalmology, Medical College of Wisconsin, Milwaukee, Wisconsin, USA

[4]Department of Biophysics, Medical College of Wisconsin, Milwaukee, Wisconsin, USA

Abstract

Aims—To examine the practical improvement in image quality afforded by a broadband light source in a clinical setting and to define image quality metrics for future use in evaluating spectral domain optical coherence tomography (SD-OCT) images.

Methods—A commercially available SD-OCT system, configured with a standard source as well as an external broadband light source, was used to acquire 4 mm horizontal line scans of the right eye of 10 normal subjects. Scans were averaged to reduce speckling and multiple retinal layers were analysed in the resulting images.

Results—For all layers there was a significant improvement in the mean local contrast (average improvement by a factor of 1.66) when using the broadband light source. Intersession variability was shown not to be a major contributing factor to the observed improvement in image quality obtained with the broadband light source. We report the first observation of sublamination within the inner plexiform layer visible with SD-OCT.

Conclusion—The practical improvement with the broadband light source was significant, although it remains to be seen what the utility will be for diagnostic pathology. The approach presented here serves as a model for a more quantitative analysis of SD-OCT images, allowing for more meaningful comparisons between subjects, clinics and SD-OCT systems.

INTRODUCTION

Optical coherence tomography (OCT) is a non-invasive tool that affords cross-sectional imaging of the living human retina (for review, see Drexler[1]). Since the introduction of the first commercial instrument to the ophthalmic community more than 12 years ago, there has

Correspondence to Dr Joseph Carroll, Medical College of Wisconsin, The Eye Institute, 925 N. 87th Street, Milwaukee, WI 53226, USA; jcarroll@mcw.edu.
HT and AMD contributed equally to this work.

Patient consent Obtained.

Competing interests None declared.

Ethics approval The study followed the tenets of the Declaration of Helsinki and was approved by the Children's Hospital of Wisconsin Institutional Review Board.

Provenance and peer review Not commissioned; externally peer reviewed.

been exponential growth in its clinical application, coinciding with the development of spectral domain OCT (SD-OCT). In parallel to the commercial deployment of SD-OCT systems, a number of groups have demonstrated methods for improving the resolution of SD-OCT. These include simply averaging multiple frames to increase the signal-to-noise ratio,[23] employing adaptive optics to compensate for the eye's monocular aberrations,[4–8] using high-speed detection to reduce motion artefacts,[9–12] and integration of broadband light sources.[13–15] Some of these research devices are reported to achieve axial resolution of nearly 2 μm in vivo. Nevertheless, the evaluation of SD-OCT images remains largely qualitative.

There is a need to evaluate image quality objectively and quantitatively. This would be useful in comparing images across different imaging systems, or in monitoring image quality over time as selective degradation of specific retinal layers may indicate early pathology. The outer retinal complex has been of particular interest, as it consists of at least five distinct layers originating from the photoreceptors and retinal pigment epithelium.[16] We define image quality using two parameters: the resolution in the image and the contrast of individual retinal layers. Depending on the clinical application, one parameter may be more useful than the other. To date, the literature has focused largely on qualitative assessments of image quality (although see Stein *et al*[17]), making it difficult to compare data sets quantitatively across instruments or to assess image quality objectively within a clinical database on a single instrument.

We compared macular SD-OCT image quality using both a broadband superluminescent diode source and standard light source in a commercially available SD-OCT. We implemented two metrics that can be useful in evaluating image quality as a step towards more quantitative treatment of clinical OCT data. We anticipate the development of additional image analysis tools as research use of SD-OCT becomes more widespread.

MATERIALS AND METHODS

Subjects

Imaging was performed in the right eye of 10 normal subjects (six male, four female), ranging in age from 24 to 40 years old with a mean of 28.4 years. Ophthalmic examination revealed no obvious abnormalities, although six of the subjects had moderate refractive errors. A Zeiss IOL Master (Carl Zeiss Meditec, Dublin, California, USA) was used to measure axial length of each eye, and nominal 4 mm horizontal OCT scans through the macula of each subject were corrected for inter-individual differences in axial length, based on Leung *et al*.[18] Axial length in our subjects ranged from 23.33 to 27.49 mm; actual macular scan lengths ranged from 3.89 to 4.58 mm.

Image acquisition

Spectral-domain OCT imaging was performed using a Bioptigen SD-OCT instrument (Bioptigen, Research Triangle Park, North Carolina, USA). Subjects were instructed to fixate on a central fixation target and 4 mm horizontal line scans were acquired through the centre of fixation, roughly corresponding to the foveal centre. Each B-scan comprised 1000 A-scans, and 100 B-scans were obtained in each scan set. Images were obtained with one of two light sources, either a broadband light source (central wavelength 878.4 nm, 186.3 nm bandwidth) or a standard source (central wavelength 860 nm, 53.7 nm bandwidth).

The theoretical axial resolution in OCT is inversely proportional to the spectral bandwidth of the light source, as given by equation 1.

$$\text{Axial resolution } (\mu) = \frac{2\ln(2)}{n\pi} \times \frac{\lambda^2}{\Delta\lambda} \quad (1)$$

The λ and $\Delta\lambda$ are the centre wavelength and bandwidth, respectively, of the light source used for imaging and n is the assumed refractive index of the tissue, 1.333. The theoretical axial resolution is 1.4 μm for the broadband source and 4.6 μm for the standard source. The power of the two sources was matched as close as possible using a 50/50 power splitter on the broadband source. The measured power at the cornea was 746 μW for the broadband configuration and 755 μW for the standard source, both below the maximum permissible exposure for this wavelength and optical configuration.[19]

Previous work has shown that speckle noise in OCT images can be reduced by averaging multiple registered B-scans together.[23] The same principle was applied with SD-OCTscans acquired in this study to maximise image quality. Scans were directly exported from the OCT machine and read into ImageJ[20] (National Institutes of Health, Bethesda, Maryland, USA) for processing. Frames from scans that were distorted due to large saccades or eye blinks were removed. Then a rigid body registration using the ImageJ plugin 'StackReg'[21] was applied to generate a stabilised frame sequence for subsequent averaging. For any given subject, the same number of frames was used to generate averaged images for the broadband and standard light sources. For one subject we used 25 frames to generate each image, for another we used 52 frames, and for the other eight we used 40 frames from each scan set.

Standard versus broadband light source

Two 4 mm horizontal OCT scan sets were acquired (each consisting of 100 B-scans), first using the broadband light source (central wavelength 878.4 nm, 186.3 nm bandwidth) and then the standard source (central wavelength 860 nm, 53.7 nm bandwidth). This sequence was repeated a second time, for a total of four scans per eye. Switching between sources took approximately 5 min. Each scan was exported into ImageJ and a single registered average image was generated for each scan set as described above. Visual inspection and then quantitative mapping of the inner limiting membrane (ILM) contour[22] was done for each subject to confirm that their broadband and standard-source images were acquired from the same retinal location. It was estimated that the scans between sessions deviated by less than 50 μm in retinal location, which is the distance between two adjacent B scans.

To compare image quality achieved using the standard and broadband light sources, the peak-to-trough ratio and local contrast of five hyper-reflective retinal layers, ILM, external limiting membrane (ELM), inner segment (IS)/outer segment junction (OS) and two retinal pigment epithelium layers, were evaluated for all four averaged images. First, longitudinal reflectivity profiles (LRP)[23] were generated at three locations along each averaged scan: the foveal centre, 0.8 mm temporal to the fovea and 0.8 mm nasal to the fovea. Each LRP used for analysis was an average of the five surrounding A-scans at each of the three locations, so these were perpendicular to the total image. From the LRP the local contrast was computed for the above five layers of interest. We define local contrast as a normalised measure of the contrast of a reflective layer, as given by equation 2.

$$\text{Local contrast} = (\text{signal of layer peak} - \text{mean signal of neighbouring troughs}) / (\text{signal of layer peak}) \quad (2)$$

The signal of the neighbouring troughs for each layer of interest was computed as an average of the neighbouring lower-reflecting layers in the OCT image (using the absolute local minimum). For example, for the ILM, the neighbouring layer trough signal comes from the vitreous and either the outer nuclear layer for the foveal measurement, or the

ganglion cell layer for the nasal and temporal measurements. For the ELM, the neighbouring layer trough signal comes from an average of the outer nuclear layer and the inner segment layer. The reported value of local contrast for each layer is an average of the measured contrast for the two averaged images for the broad-band and standard source imaging conditions.

The improvement in resolution was evaluated by comparing the full-width half-height (FWHH) of the ELM layer in the registered and averaged images generated by the standard and broadband light sources. Using ImageJ, five plot profiles, drawn perpendicular through the ELM in the temporal retina, were averaged together. The averaged profiles were fit to a Gaussian function in order to objectively compute FWHH for each of the two light sources. Resolution was computed from the average image created from one broadband scan set and one standard-source scan set for each subject.

Evaluating intersession variability

In order to constrain the contribution of intersession variability to any observed differences between the two light sources, we did a control experiment on one subject. Using the broadband light source, an OCTscan was obtained on one subject every 2 h for 48 h. A registered average image was generated from each scan, using 30 frames from each scan set. The local contrast was then analysed as described above to evaluate layer contrast as a function of time.

RESULTS

Improvement in image quality and resolution using broadband light source

As has been observed by others,[23] the use of multiple frames produces an image with reduced speckle noise, and these averaged images were what we used for subsequent analysis. To visualise the improvement in image quality afforded by the use of the broadband light source, we obtained images of the same retina using the two different light sources (figure 1). While the image intensity appeared lower and may be judged as a lower quality image based on a metric-like signal strength, there was a marked improvement in the contrast of the retinal layers. This is visualised by inspecting an LRP from the same retinal region in both images (figure 1), with the peaks of the highly reflecting layers being more easily resolved from the neighbouring layers. To quantify this improvement in image quality, the mean local contrast for five hyper-reflective retinal layers was calculated. For all layers, a significant improvement in the mean local contrast (figure 2A) was present, with an average improvement by a factor of 1.66 seen when using the broadband light source (range 1.17–2.14).

In addition to an improved image contrast, an improvement in resolution was also observed in the plot profiles taken through the ELM. The FWHH of the ELM was reduced on average by a factor of 1.9 across subjects (range 1.58–2.35) when using the broadband light source (data not shown).

In order to assess whether the difference between light sources could be affected by low repeatability of the scan protocol, one subject was imaged every 2 h for 48 h. The same image analysis was performed on these images and image quality was found to be remarkably stable, assessed by monitoring layer contrast as a function of time (figure 2B). It is important to note that while every effort was made to ensure the exact same retinal location was scanned each time (through visual inspection and quantitative mapping of the ILM contour[22]), there could be residual errors in scan location. The mean local contrast for any given layer varies by about 11% over the entire experiment, suggesting that intersession

variability was not a major contributing factor to the observed improvement in image quality obtained with the broadband light source.

Visualisation of IPL lamination

Visual signals are transferred from the photoreceptor cells to the retinal ganglion cells via bipolar cells. There are nearly a dozen different types of bipolar cell involved in this process, and the major distinguishing feature of the cone bipolar cells is the level of stratification of their axons within the inner plexiform layer (IPL). The IPL is where bipolar cells and ganglion cells form their synapses. When using the broadband source, an interesting sublamination of the IPL was observed (figure 3A). These horizontal striations were present in nearly all the images generated with the broadband light source, and are reminiscent of the laminar organisation of the IPL observed in monkey (figure 3C)[24] and mouse retina (figure 3B).[2526] These striations reflect the fact that synapses aggregate in discrete layers within the IPL.

DISCUSSION

The combination of a high-resolution, efficient and clinic-friendly OCT system with robust image processing techniques represents a significant advance over existing commercially available SD-OCTsystems. We have shown that a commercially available SD-OCT instrument equipped with a broadband light source can provide improved contrast and resolution of outer retinal layers. A local contrast analysis demonstrated an improved contrast of the retinal layers as well as better resolution of the IS/OS layer, as seen by a narrower FWHH when using the broadband light source.

The approach presented here can serve as a model for a more quantitative analysis of OCT images, allowing for meaningful comparisons between subjects, clinics, and OCTsystems. Rather than place qualitative labels on the image and/or devices such as ‘super’, ‘ultra’, ‘high’ or ‘low’, a more quantitative description of image quality is within reach and would go a long way to help clinicians to make decisions about which imaging tool best fits their needs. This is especially relevant as additional technological advances are made in SD-OCT.

Horizontal striations within the IPL were also observed and are believed to represent synaptic sublamination. In most SD-OCT images it is possible to discriminate the nerve fibre layer from the ganglion cell layer and the ganglion cell layer from the IPL. This IPL sublamination has not previously been observed using the standard source or two other commercial SD-OCT systems in our clinic. It would be interesting to examine this lamination in patients with advanced photoreceptor degeneration, as one might be able to visualise downstream disruptions in retinal circuitry known to occur after a loss of photoreceptor input.[27]

As stated earlier, the axial resolution in OCT is inversely related to the bandwidth of the imaging light source. Thus, an improvement in resolution is expected between the two light sources by a factor of about 3.2. However, it was observed that the FWHH of the ELM decreased by only a factor of 2. Probably the biggest factor preventing the realisation of the full theoretical benefit of the broadband light source is that the human eye is wrought with chromatic aberration. The predicted change in focus for our broadband light source (λ_{max}=878.4 nm, $\Delta\lambda$=186.3 nm) is nearly 0.5 D.[28] Further improvement in resolution approaching the theoretical improvement could be realised by implementing an achromatising lens to compensate for the eye’s chromatic aberration.[29] In addition, the spectrometer in the system is calibrated for the narrow band source and thus the benefit of deeper penetration of the longer wavelengths is not fully captured when using the broadband source.

Last, there are additional advances in clinical OCT imaging on the horizon. Adaptive optics has also been shown to increase the resolution of OCT by correcting for the eye's monochromatic aberrations,[4578] making it possible to visualise individual cone photoreceptors in the outer retina. However, recently it has been shown that simply increasing the speed of the line scan camera can mitigate the effects of retinal motion and enable visualisation of the peripheral cone mosaic.[12] Systems incorporating both high-speed and adaptive optic correction of the eye's aberrations would provide even better resolution. Nevertheless, these advances are not currently commercially available in the form of a clinical imaging system. Quantitative analyses such as those described here will be useful in determining the benefit of advanced technology as it becomes available.

Acknowledgments

The authors thank B. Bower, E. Buckland and E. Schneider (Bioptigen, Inc., Research Triangle Park, North Carolina, USA) for assistance with instrument calibration and for helpful comments on the manuscript.

Funding The authors acknowledge grant support from the National Institutes of Health (EY001931, EY014537 and EY017607) and from the Gene & Ruth Posner Foundation, Fight for Sight, The E. Matilda Ziegler Foundation for the Blind, the RD & Linda Peters Foundation, Hope for Vision, and an unrestricted grant from Research to Prevent Blindness. Joseph Carroll is the recipient of a Career Development Award from Research to Prevent Blindness.

References

1. Drexler W. Ultrahigh-resolution optical coherence tomography. J Biomed Opt. 2004; 9:47–74. [PubMed: 14715057]
2. Sander B, Larsen M, Thrane L, et al. Enhanced optical coherence tomography imaging by multiple scan averaging. Br J Ophthalmol. 2005; 89:207–12. [PubMed: 15665354]
3. Jørgensen TM, Thomadsen J, Christensen U, et al. Enhancing the signal-to-noise ratio in ophthalmic optical coherence tomography by image registration-method and clinical examples. J Biomed Opt. 2007; 12:041208. [PubMed: 17867797]
4. Hermann B, Fernández EJ, Unterhuber A, et al. Adaptive-optics ultrahigh-resolution optical coherence tomography. Opt Lett. 2004; 29:2142–4. [PubMed: 15460883]
5. Fernández EJ, Považay B, Hermann B, et al. Three-dimensional adaptive optics ultrahigh-resolution optical coherence tomography using a liquid crystal spatial light modulator. Vision Res. 2005; 45:3432–44. [PubMed: 16249013]
6. Merino D, Dainty C, Bradu A, et al. Adaptive optics enhanced simultaneous en-face optical coherence tomography and scanning laser ophthalmoscopy. Opt Express. 2006; 14:3345–53. [PubMed: 19516479]
7. Zhang Y, Cense B, Rha J, et al. High-speed volumetric imaging of cone photoreceptors with adaptive optics spectral-domain optical coherence tomography. Opt Express. 2006; 14:4380–94. [PubMed: 19096730]
8. Pircher M, Zawadzki RJ, Evans JW, et al. Simultaneous imaging of human cone mosaic with adaptive optics enhanced scanning laser ophthalmoscopy and high-speed transversal scanning optical coherence tomography. Opt Lett. 2008; 33:22–4. [PubMed: 18157245]
9. Wojtkowski M, Leitgeb R, Kowalczyk A, et al. In vivo human retinal imaging by Fourier domain optical coherence tomography. J Biomed Opt. 2002; 7:457–63. [PubMed: 12175297]
10. White B, Pierce M, Nassif N, et al. In vivo dynamic human retinal blood flow imaging using ultra-high-speed spectral domain optical coherence tomography. Opt Express. 2003; 11:3490–7. [PubMed: 19471483]
11. Leitgeb RA, Drexler W, Unterhuber A, et al. Ultrahigh resolution Fourier domain optical coherence tomography. Opt Express. 2004; 12:2156–65. [PubMed: 19475051]
12. Potsaid B, Gorczynska I, Srinivasan VJ, et al. Ultrahigh speed spectral/Fourier domain OCT ophthalmic imaging at 70,000 to 312,500 axial scans per second. Opt Express. 2008; 16:15149–69. [PubMed: 18795054]

13. Drexler W, Morgner U, Kartner FX, et al. In vivo ultrahigh-resolution optical coherence tomography. Opt Lett. 1999; 24:1221–3. [PubMed: 18073990]
14. Drexler W, Morgner U, Ghanta RK, et al. Ultrahigh-resolution ophthalmic optical coherence tomography. Nat Med. 2001; 7:502–7. [PubMed: 11283681]
15. Wojtkowski M, Srinivasan V, Ko T, et al. Ultrahigh-resolution, high-speed, Fourier domain optical coherence tomography and methods for dispersion compensation. Opt Express. 2004; 12:2404–22. [PubMed: 19475077]
16. Srinivasan VJ, Monson BK, Wojtkowski M, et al. Characterization of outer retinal morphology with high-speed, ultrahigh-resolution optical coherence tomography. Invest Ophthalmol Vis Sci. 2008; 49:1571–9. [PubMed: 18385077]
17. Stein DM, Ishikawa H, Hariprasad R, et al. A new quality assessment parameter for optical coherence tomography. Br J Ophthalmol. 2006; 90:186–90. [PubMed: 16424531]
18. Leung CK, Cheng ACK, Chong KKL, et al. Optic disc measurements in myopia with optical coherence tomography and confocal scanning laser ophthalmoscopy. Invest Ophthalmol Vis Sci. 2007; 48:3178–83. [PubMed: 17591887]
19. Institute ANS. American National Standard for safe use of lasers: ANSI Z136.1-2007. Orlando (FL): Laser Institute of America; 2007. p. 276
20. Abramoff MD, Magelhaes PJ, Ram SJ. Image processing with ImageJ. Biophotonics International. 2004; 11:36–42.
21. Thévenaz P, Ruttimann UE, Unser M. A pyramid approach to subpixel registration based on intensity. IEEE Trans Image Process. 1998; 7:27–41. [PubMed: 18267377]
22. Dubis A, McAllister JT, Carroll J. Reconstructing foveal pit morphology from optical coherence tomography imaging. Br J Ophthalmol. Published Online First: 26 May 2009. 10.1136/bjo.2008.150110
23. Huang Y, Cideciyan AV, Papastergiou GI, et al. Relation of optical coherence tomography to microanatomy in normal and rd chickens. Invest Ophthalmol Vis Sci. 1998; 39:2405–16. [PubMed: 9804149]
24. Haverkamp S, Haeseleer F, Hendrickson AE. A comparison of immunocytochemical markers to identify bipolar cell types in human and monkey retina. Vis Neurosci. 2003; 20:589–600. [PubMed: 15088712]
25. Wässle H. Parallel processing in the mammalian retina. Nat Rev Neurosci. 2004; 5:747–57. [PubMed: 15378035]
26. Haverkamp S, Wässle H. Immunocytochemical analysis of the mouse retina. J Comp Neurol. 2000; 424:1–23. [PubMed: 10888735]
27. Jones BW, Marc RE. Retinal remodeling during retinal degeneration. Exp Eye Res. 2005; 81:123–37. [PubMed: 15916760]
28. Fernández EJ, Unterhuber A, Prieto PM, et al. Ocular aberrations as a function of wavelength in the near infrared measured with a femtosecond laser. Opt Express. 2005; 13:400–9. [PubMed: 19488366]
29. Fernández EJ, Unterhuber A, Považay B, et al. Chromatic aberration correction of the human eye for retinal imaging in the near infrared. Opt Express. 2006; 14:6213–25. [PubMed: 19516794]
30. Gloesmann M, Hermann B, Schubert C, et al. Histologic correlation of pig retina radial stratification with ultrahigh-resolution optical coherence tomography. Invest Ophthalmol Vis Sci. 2003; 44:1696–703. [PubMed: 12657611]
31. Pianta MJ. A more coherent relationship between optical coherence tomography scans and retinal anatomy. Clin Exp Optom. 2008; 91:327–9. [PubMed: 18399805]

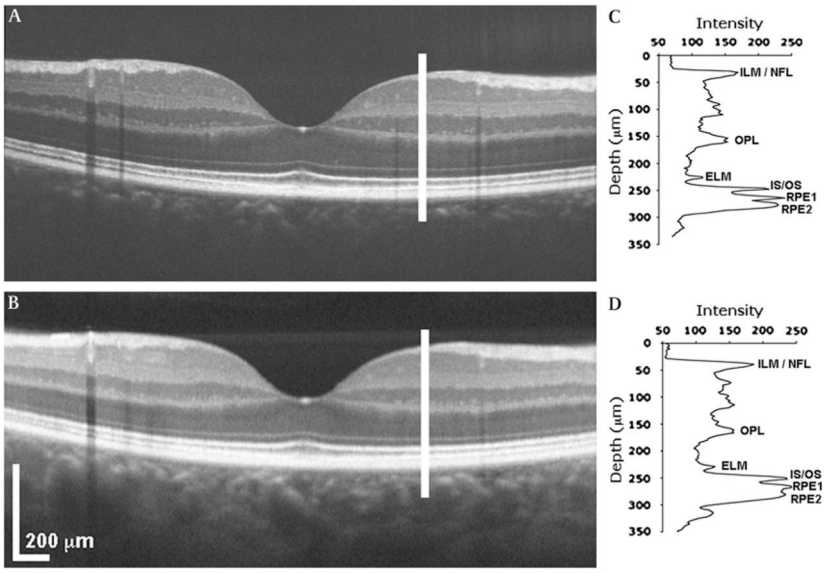

Figure 1.

Imaging the retina with a broadband light source. Registered and averaged images of the retina from a 27-year-old woman obtained with the broadband light source (A) and the standard optical coherence tomography (OCT) light source (B). Despite a slight reduction in image intensity, contrast is improved when using the broadband light source. Longitudinal reflectivity profiles (LRPs) obtained at the white vertical line for the broadband (C) and standard source (D) images. In the OCT images, the grey scale represents signal amplitude —low reflecting layers indicate nuclear layers while high reflectivity typically comes from synaptic layers in the healthy retina. ELM, external limiting membrane; ILM, inner limiting membrane; IS/OS, inner segment/outer segment junction; NFL, nerve fibre layer; OPL, outer plexiform layer; RPE, retinal pigment epithelium. Assignment of layers is based on literature consensus.[163031]

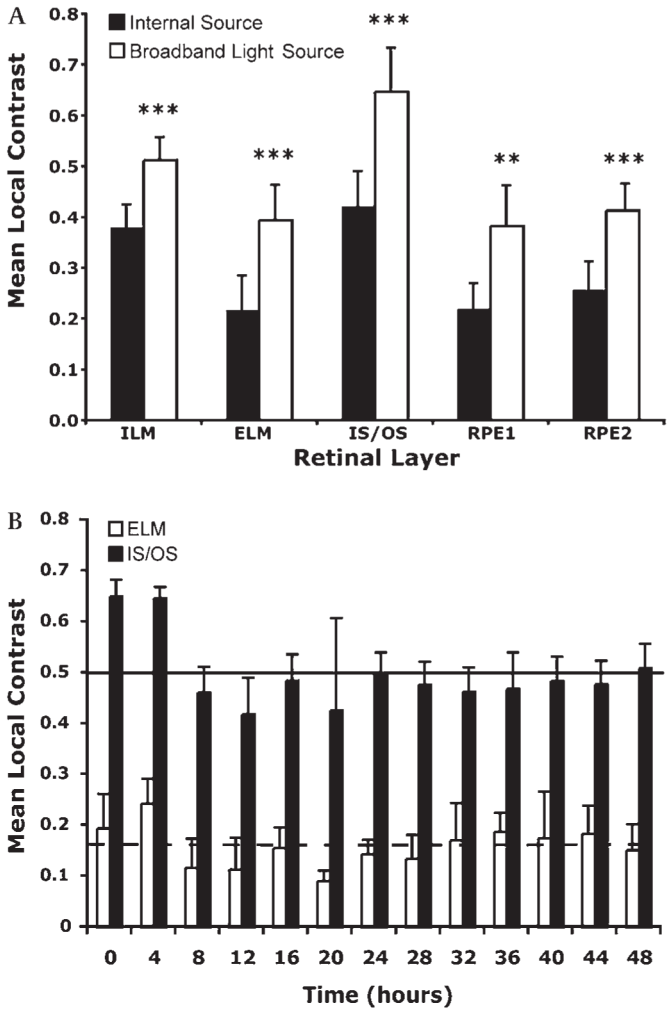

Figure 2.

Improved resolution of retinal layers with the broadband source. (A) To quantify the improvement in image quality, we calculated mean local contrast for five retinal layers (inner limiting membrane (ILM), external limiting membrane (ELM), inner segment/outer segment junction (IS/OS), retinal pigment epithelium (RPE) 1, RPE2). For all layers, there was a significant improvement in contrast (paired t test): **p=0.0001, ***p<0.0001. Error bars represent one SD of the 10 subjects. (B) Layer contrast for the ELM (white bars) and IS/OS (black bars) over a 48 h experiment where the same retina was imaged every 2 h. Layer contrast was computed for all layers. The local contrast deviated from the mean by 12.3% for the ILM, 16.6% for the ELM, 8% for the IS/OS, 10.6% for RPE1, and 10.7% for RPE2. Error bars represent one standard deviation, determined from the nasal, foveal and temporal data points at each time point for this single retina.

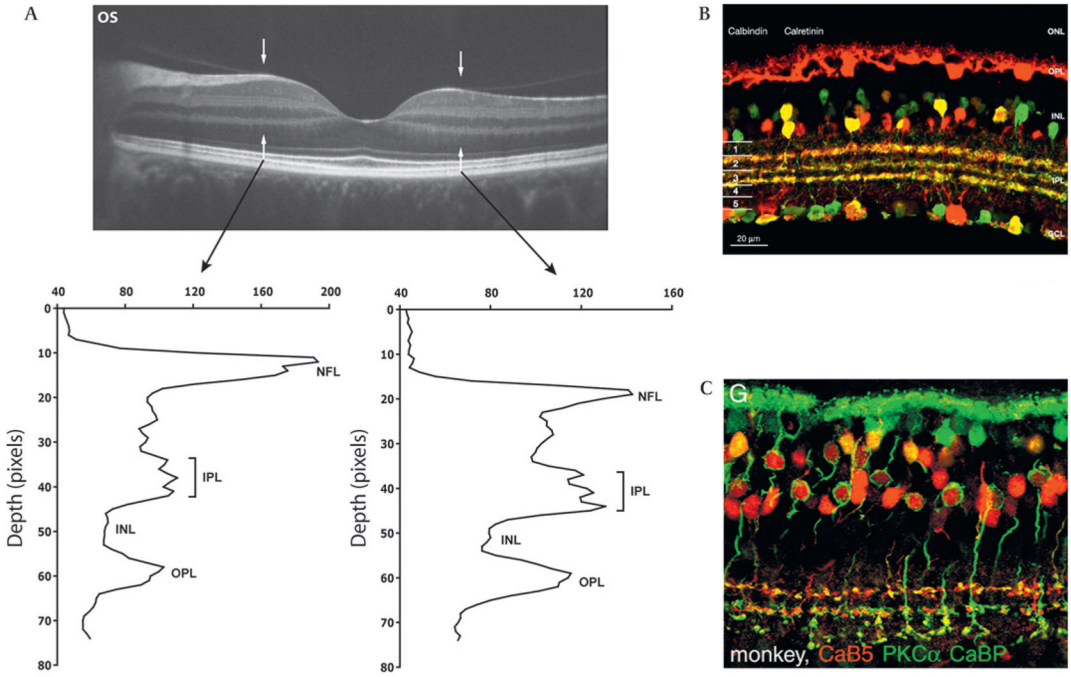

Figure 3.

Visualisation of inner plexiform layer (IPL) sublamination. (A) Registered average of 60 B scans (broadband source). The IPL sublamination is visible as three bright bands and two darker bands: this is easily seen in the longitudinal reflectivity profiles (LRPs) taken between the two sets of arrowheads. For comparison, immunostained mouse[25] (B) and monkey[24] (C) retinas showing the stratification of the IPL are shown (images reproduced with permission). INL, inner nuclear layer; OPL, outer plexiform layer.